A Conserved Histidine in Vertebrate-Type Ferredoxins Is Critical for Redox-Dependent Dynamics†

Milka Kostic,‡ Rita Bernhardt,§ and Thomas C. Pochapsky*,‡

Department of Chemistry, Brandeis University, 415 South Street, MS 015, Waltham, Massachusetts 02451, and FR 8.8 Biochemie, Universität des Saarlandes, Postfach 151150, D-66041, Saarbrücken, Germany

Received March 28, 2003; Revised Manuscript Received May 16, 2003

ABSTRACT: Adrenodoxin (Adx) belongs to the family of $Cys_4Fe_2S_2$ vertebrate-type ferredoxins that shuttle electrons from NAD(P)H-dependent reductases to cytochrome P450 enzymes. The vertebrate-type ferredoxins contain a conserved basic residue, usually a histidine, adjacent to the third cysteine ligand of the $Cys_4Fe_2S_2$ cluster. In bovine Adx the side chain of this residue, His 56, is involved in a hydrogen-bonding network within the domain of Adx that interacts with redox partners. It has been proposed that this network acts as a mechanical link between the metal cluster binding site and the interaction domain, transmitting redox-dependent conformational or dynamical changes from the cluster binding loop to the interaction domain. H/D exchange studies indicate that oxidized Adx (Adx^o) is more dynamic than reduced Adx (Adx^r) on the kilosecond time scale in many regions of the protein, including the interaction domain. Dynamical differences on picosecond to nanosecond time scales between the oxidized (Adx^o) and reduced (Adx^r) adrenodoxin were probed by measurement of ^{15}N relaxation parameters. Significant differences between ^{15}N R_2 rates were observed for all residues that could be measured, with those rates being faster in Adx^o than in Adx^r. Two mutations of His 56, H56R and H56Q, were also characterized. No systematic redox-dependent differences between ^{15}N R_2 rates or H/D exchange rates were observed in either mutant, indicating that His 56 is required for the redox-dependent behavior observed in WT Adx. Comparison of chemical shift differences between oxidized and reduced H56Q and H56R Adx confirms that redox-dependent changes are smaller in these mutants than in the wild-type Adx.

The oxidative conversion of cholesterol to pregnenolone in mitochondria of the adrenal cortex marks the beginning of steroid hormone biosynthesis. Cytochrome $P\text{-}450_{scc}$ (CYP11A1) catalyzes this three-step oxidation. Cholesterol is first converted to 22(*R*)-hydroxycholesterol, which is further oxidized to 20,22-dihydroxycholesterol and finally to pregnenolone and 4-methylpentanal. Each oxidation requires a molecule of O_2 and two electrons. The electrons required are ultimately derived from the oxidation of NADPH, which is catalyzed by the flavoenzyme, adrenodoxin reductase (AdR).[1] AdR reduces the $Cys_4Fe_2S_2$ ferredoxin Adx, which acts as a single-electron shuttle from AdR to CYP11A1. Besides CYP11A1, bovine Adx is the reductant of another cytochrome P-450 enzyme, $P\text{-}450_{11\beta}$ (CYP11B1). This enzyme catalyzes the 11β- and C-18 hydroxylation of steroids, leading to formation of cortisol and aldosterone. All three components of the electron-transfer chain are located on the matrix side of the inner mitochondrial membrane, mostly in the adrenal cortex, although they can be found in the mitochondria of some other tissues as well (*1*). The cognate P450s of the soluble Adx are membrane-bound enzymes, and adrenodoxin reductase (AdR) is membrane associated.

There are several proposed models for electron transport in this system. The most widely accepted is the shuttle model, wherein Adx acts as a mobile shuttle between AdR and cytochrome P450 (*2*, *3*). Recently, it was observed that Adx forms dimers when oxidized, which lead to another model for electron transfer (*4*) in which oxidized Adx (Adx^o) binds to the AdR as a dimer. A single electron is transferred from AdR to the directly bound Adx and then to the second Adx molecule. Upon reduction, reduced Adx (Adx^r) dissociates, and the second electron is transferred from AdR to Adx, which dissociates from AdR upon reduction. Both Adx^r monomers transfer one electron each to the cytochrome P450 and then redimerize. It has been pointed out that the mechanism of electron transfer might differ from one mitochondrial P450 system to another (*5*).

Adx is the archetype of the family of vertebrate-type ferredoxins. Mature bovine Adx consists of 128 amino acid residues and is negatively charged at physiological pH. It contains a single Fe_2S_2 cluster ligated by four cysteinyl thiolate ligands, Cys 46, Cys 52, Cys 55, and Cys 92. The metal cluster cycles between two oxidation states, Fe(III)/Fe(III) and Fe(II)/Fe(III). Crystal structures of a C-terminal

† This work was supported by a grant from the National Institutes of Health (RO1-GM44191 to T.C.P.) and by a grant from the Deutsche Forschungsgemeinschaft (Be 1343/12-1 to R.B.).

* To whom correspondence should be addressed. Phone: (781) 736-2559. Fax: (781) 726-2516. E-mail: pochapsk@brandeis.edu.

‡ Brandeis University.

§ Universität des Saarlandes.

[1] Abbreviations: Adx, adrenodoxin; DTT, dithiothreitol; HSQC, heteronuclear single-quantum coherence; IPTG, isopropyl β-D-thiogalactoside; LB, Luria−Bertani media; NMR, nuclear magnetic resonance; NOE, nuclear Overhauser effect; NOESY, NOE spectroscopy; TOCSY, total correlation spectroscopy; WT, wild type; Adx^o, oxidized adrenodoxin; Adx^r, reduced adrenodoxin; RMSD, root mean square deviation; 2D, two dimensional; Pdx, putidaredoxin; Fdx, ferredoxin; AER, atomic element radius; AdR, adrenodoxin reductase; OD, optical density.

10.1021/bi034500r CCC: $25.00
Published on Web 06/19/2003

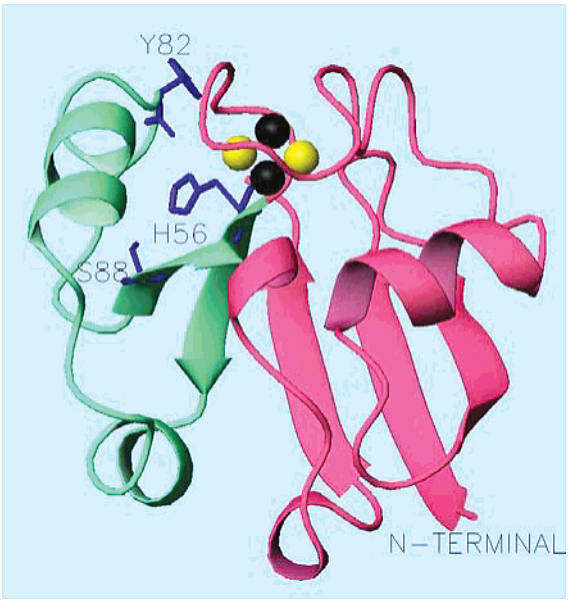

FIGURE 1: Ribbon representation of the crystal structure of oxidized Adx (*6*). The hydrophobic core, with characteristic β-grasp motif, is given in red, and the interaction domain is in green. The Fe_2S_2 cluster, located at the edge of hydrophobic core, is represented with four spheres. Fe atoms are given in black and S atoms in yellow. Three residues that form the hydrogen-bonding network proposed to play a critical role in transmitting redox-dependent changes from the cluster binding loop to the interaction domain, His 56, Tyr 82, and Ser 88, are shown in blue. The figure is made using MOLMOL (*42*).

truncated bovine Adx^o (4−108) (*6*) and full-length bovine Adx^o (*7*) have been determined. Recently, NMR structures of full-length Adx^o and Adx^r have been published (*4*). The Adx structure is organized into two domains, a hydrophobic core (residues 5−55 and 91−108) and an interaction domain (residues 56−90), so-called because many of the residues important for interactions with redox partners are found in this domain (Figure 1) (*8*). The metal cluster binding site is located close to the surface of the protein between the two domains. The hydrophobic core of Adx folds into a β-grasp motif often referred to as the ubiquitin superfold (*9*). This fold is highly conserved in the ferredoxin superfamily, which includes vegetative and bacterial ferredoxins. On the other hand, the interaction domain is more variable within the ferredoxin superfamily.

Like other vertebrate-type ferredoxins, Adx exhibits considerable differences in local dynamics as a function of oxidation state (*4*, *10*). Redox-dependent affinity of Adx for AdR has been observed (*11*, *12*). It was determined that Adx^o binds about 20 times more tightly to AdR than Adx^r, consistent with the direction of electron transfer. Unlike the related ferredoxin putidaredoxin (Pdx), in which redox-dependent binding is proposed to modulate interactions with cytochrome $P450_{cam}$ (*13*), redox dependence of Adx binding to cytochrome P450 is less pronounced (*11*, *12*).

Several regions of Adx exhibit redox-dependent changes as measured by local chemical shift and dynamic perturbations. These include the interaction domain, the C-terminal peptide, and regions structurally and/or sequentially adjacent to the metal cluster binding loop. The largest redox-dependent chemical shift changes in Adx are observed for C-terminal residues (*4*). The 17 C-terminal residues of Adx are disordered in the crystal structure of the full-length protein and in both NMR structures (*4*, *7*). Although it has been proposed that the C-terminal peptide plays a role in modulating the electron-transfer properties of the molecule and has been shown to be important for dimerization of Adx, C-terminal truncation mutants of Adx, in general, exhibit greater activity than the wild type (*12*). Besides the C-terminal peptide, significant redox dependence of chemical shifts is observed for residues 38, 57, 75, 81−83, and 95 (*4*). Many of these residues are found in the interaction domain, and it is of some interest to determine how redox-dependent perturbations are transmitted from the metal cluster to the interaction domain. Sequence alignment of vertebrate-type ferredoxins reveals the presence of a conserved basic residue immediately following the third cysteine ligating the metal center (Cys 55 in Adx). This residue (usually a histidine, although arginine is found in this position in some vertebrate-type ferredoxins) provides mechanical linkage between the metal cluster binding loop and the interaction domain (*14*, *15*). The crystallographic structure of Adx shows that the imidazole ring of His 56 takes part in a hydrogen-bonding network within the interaction domain. At physiological pH, only the imidazole $N^{\delta 1}$ of His 56 is protonated, and the imidazole is electrically neutral (*16*). The His 56 $H^{\delta 1}$ is hydrogen bonded to the carbonyl of Tyr 82, while the unprotonated $N^{\epsilon 2}$ is within hydrogen-bonding distance of Ser 88 hydroxyl H^{γ}. A similar hydrogen-bonding network has been identified in putidaredoxin (Pdx) (*16*) and in an *E. coli* ferredoxin (Fdx) (*17*). Modification of His 56, either through chemical modification or mutagenesis, reduces the affinity of Adx for its redox partners (*18*). Bernhardt and co-workers mutated His 56 in bovine Adx to Gln, Thr, and Arg (*19*). All three mutant proteins have lower affinities for both AdR and cytochrome P450, lower conformational stabilities, and higher reduction potentials than wild-type (WT) Adx. We now report results of structural and dynamical comparison of WT, H56Q, and H56R Adx in both oxidation states. Our results confirm that His 56 is a crucial link in transmitting redox-dependent conformational and dynamic effects from the metal binding loop to the interaction domain of Adx.

MATERIALS AND METHODS

Protein Expression and Purification. The methodology used to construct the H56Q and H56R mutants of bovine Adx has been described previously (*20*). WT and mutant Adx proteins were expressed in *Escherichia coli* strain BL21-(DE3)pLysS by induction of T7 RNA polymerase production with IPTG. Cells were made electrocompetent and transformed with the appropriate plasmid construct 1 day prior to cell culture for expression. Transformed cells were allowed to grow on LB plates containing 200 μg/mL ampicilin (amp) and 34 μg/mL chloramphenicol (chl) overnight at 37 °C. Individual colonies were used to inoculate 5 mL cultures in LB containing the same amounts of amp and chl as the LB plates. After 4 h at 37 °C, cells were transferred either to 50 mL of the LB/amp/chl mixture or to 50 mL of a minimal medium (M9) containing the same concentrations of amp and chl as mentioned above, depending whether production of unlabeled or labeled sample was desired. After an additional 3 h cells were transferred to 1 L of the appropriate medium supplemented with amp and chl. For ^{15}N-labeled samples, M9 medium was prepared using 1 g of $^{15}NH_4Cl$

(Cambridge Isotope Laboratories) per liter as sole nitrogen source. Regardless of the medium used, cell cultures were induced with IPTG (final concentration of 1 mM) after reaching 0.8−1.0 optical density at 600 nm. Cells were harvested after 16−20 h of growth after induction. In general, cell paste yields were 4−8 g/L of medium. WT, H56R, and H56Q bovine Adx were all expressed as holoproteins, with intact metal clusters.

The cell paste was suspended in 25 mL of lysis buffer [50 mM Tris-HCl (pH 8.0), 1 mM DTT, 1.8 mg of DNase I, 1.8 mg of RNase A, 10 mg of lysozyme, and 10 mg of tosyl chloride] and stirred at room temperature for 45 min. To complete lysis, cells were sonicated and pellets removed by centrifugation. The clear supernatant was loaded onto a DEAE ion-exchange column preequilibrated with 50 mM Tris-HCl (pH 7.4) buffer. A salt gradient (0−1 M KCl) was used to elute protein from the column. Purity of fractions was determined spectrophotometrically, measuring the A_{414}/A_{276} ratio. Fractions with this ratio greater than 0.25 were collected, concentrated, and loaded onto a P30 (Bio-Rad) size exclusion column, preequilibrated with N_2-purged 50 mM Tris-HCl (pH 7.4) buffer. Fractions from the P30 column with an A_{414}/A_{276} ratio greater than 0.7 were concentrated to ~300 μL. Exchange into NMR buffer [50 mM *d*-Tris-HCl (pH 7.4) in 90/10 H_2O/D_2O mixture] was performed using a P2 (Bio-Rad) spin column. Samples were between 0.8 and 2.0 mM for NMR experiments.

Samples were reduced in a Coy anaerobic chamber under a 5% H_2/95% N_2 atmosphere. Reduction was performed prior to final buffer exchange by addition of a small excess of freshly prepared 1 M sodium dithionite solution in 1 M Tris-HCl (pH 8.0) buffer. The extent of the reduction was followed visually, since all three proteins change color from brown to ruby red upon reduction. After reduction, the sample was passed through a P2 column packed with degassed resin, equilibrated with oxygen-free NMR buffer, and kept anaerobic for several days prior to exchange. This step ensures both buffer exchange and removal of excess dithionite and oxidation products of the reduction reaction.

Samples for H/D amide proton exchange were prepared as described above, and H/D exchange was initiated by passage of the protonated sample through a short P2 (Bio-Rad) spin column preequilibrated with the appropriate deuterated buffer. In the case of reduced samples, the buffer exchange procedure was performed in the anaerobic chamber in order to prevent reoxidation of the sample.

NMR Experiments. All NMR experiments were performed on a Varian Unity Inova 500 11.74 T spectrometer, operating at 499.709 and 50.641 MHz for ^{1}H and ^{15}N, respectively. ^{1}H chemical shifts are referenced to external DSS using the ^{1}H resonance of water as the internal reference. ^{15}N chemical shifts are referenced to the ^{1}H frequency using a proportionality ratio of 0.101329118 (*21*). Coherence selection in the ^{15}N dimension of all experiments was obtained using pulsed field gradients, and sensitivity enhancement and phase sensitivity in the ^{15}N dimension were obtained using Rance−Kay acquisition and combinational processing schemes (*22*, *23*). For broad-band ^{15}N decoupling during acquisition, the GARP (*24*) composite pulse decoupling scheme was used. All NMR experiments were performed at 17 °C (290.15 K) with the probe temperature calibrated using a methanol standard (*25*).

2D ^{1}H, ^{15}N HSQC experiments were used for detection of ^{15}N T_1 and T_2 measurements, with the ^{1}H carrier frequency positioned at the water signal and the carrier frequency of ^{15}N set at 118 ppm (*26*). Spectral widths of 8082 Hz for ^{1}H and 2200 Hz for ^{15}N were used. All relaxation time measurements were carried out using 128 × 1024 complex points, with a total of 64 scans per t_1 point. For T_1 determination of WT Adx in both oxidation states, two separate runs were performed with variable delays (τ) of 20, 60, 200, 400, 600, and 900 ms and 40, 120, 250, 500, 750, and 1000 ms, respectively. For T_2 measurements of WT Adx^o, variable delays (τ) of two independent runs were 30, 50, 70, 90, 110, 150, 190, and 230 ms and 30, 50, 70, 110, 170, and 230 ms, respectively. For WT Adx^r relaxation delays were 30, 50, 70, 90, 110, 150, and 230 ms for the first run and 30, 50, 90, 130, 170, and 210 ms for the second. Both the H56Q and H56R Adx mutants were found to be less stable than the wild type in both oxidation states. Due to their decreased stability, only a single run was performed for T_1 and T_2 determination for mutant proteins. For both mutants, in both oxidation states, delays for T_1 determination were 40, 120, 300, 600, 750, and 1000 ms and for T_2 determination 10, 30, 70, 110, 150, and 210 ms. In all experiments, delay times between acquisitions were 1.5 s to ensure complete recovery of the magnetization. Relaxation parameters T_1 and T_2 were calculated by nonlinear curve fitting of measured peak intensities as a function of delay time τ. Reported T_1 and T_2 values for WT Adx in both oxidation states represent the average of two independent runs. To estimate error, the standard deviation between two independent runs and the average was calculated for each residue, and it was determined that the percent error does not exceed 3%. Since only one set of data was available for the mutants, error was estimated from the curve fitting procedure, the average determined error not exceeding 8%.

To measure ^{1}H, ^{15}N heteronuclear NOE intensities, two experiments were performed, one without and one with broad-band ^{1}H saturation during the recycle delay (*27*). In both cases the recycle delay was set to 3 s. All data sets were acquired as 128 × 1024 complex points with 16 scans per t_1 point. NOE values were determined as the ratios of peak heights in the spectrum recorded with saturation to those recorded without.

The kinetics of amide H/D exchange in WT and H56Q Adx in both oxidation states were followed by recording a series of ^{1}H, ^{15}N HSQC experiments during the course of 2 days in the case of WT and 24 h in the case of H56Q Adx. The experiments were carried out using the standard spectral widths in both dimensions, reported above, and using 64 × 1024 complex points, with total of eight scans per t_1 point. The total lag time between the start of exchange and acquisition of the first ^{1}H, ^{15}N HSQC spectrum was ~40 min. As such, exchange processes equilibrating in less than ~1 h could not be monitored. Data points were recorded every 20 min for the first 24 h (in the case of WT Adx) and for the first 12 h (in the case of H56Q Adx). After that, data were recorded every 2 h for WT and every 2 h for H56Q Adx. Rate constants for amide H/D exchange were extracted from the time dependence of peak intensities fitted to a single exponential first-order rate equation.

To characterize the structures of the two mutants, homonuclear NOESY and TOCSY experiments were performed.

A homonuclear ^{1}H NOESY spectrum was obtained using a 100 ms NOE mixing time. Two TOCSY experiments were performed with mixing times of 10 and 60 ms, to allow for detection of direct and multiple step correlations, respectively. Spectral widths in both dimensions were 8082 Hz. 2D NOESY spectra were recorded with 512 × 4096 complex points, with 30−50 scans per t_1 point. 2D TOCSY spectra, for both mixing times, were recorded as 512 × 2048 complex points with 32 scans per t_1 point. Water suppression was achieved by applying a gradient echo sequence (*28*).

Data processing and analysis were performed using the Felix 2.0 software package (Biosym Techologies, San Diego, CA) operating on a Silicon Graphics O_2 workstation. 2D NOESY and TOCSY FIDs were multiplied by a 90° shifted squared sine bell and then zero-filled. The first point of each FID was multiplied by 0.5 in order to remove baseline distortions. A polynomial baseline correction was applied in the directly detected dimension. All relaxation data and amide H/D exchange data were processed using a Gaussian window function in the directly detected dimension and a 90° shifted sine bell window function in the indirectly detected dimension. In the case of WT Adx, in both oxidation states, peaks were identified on the basis of previously published assignments (*4*). The two mutants studied show minor differences in spectral appearance. Those differences were noted, and new assignments are reported here.

Calculation of Protection Factors. On the basis of the results of amide proton exchange rate measurements, protection factors have been calculated using eq 1 for all the residues with measurable exchange rates:

$$P = k^{\mathrm{int}}/k^{\mathrm{exp}} \quad (1)$$

where P is the protection factor, k^{int} is the intrinsic exchange rate for the free peptide in the absence of any secondary structure (*29*), and k^{exp} is experimentally measured exchange rate constant. Protection factors were calculated using a corrected value of pD of 7.8 and taking into account only base-catalyzed exchange. Application of eq 1 for protection factor calculation is valid under native conditions, and the system studied here satisfies that requirement.

Molecular Modeling. His 56 was replaced in the published structure of Adx (*6*) by Arg and Gln using the Biopolymer module of InsightII 2000 (MSI, San Diego). Mutant structures were energy minimized using 100 steps of steepest descent prior to 2000 steps of conjugate gradient energy minimization. The output structure from minimization procedure was further used as input for room temperature molecular dynamics (MD) simulations. The first stage was 5 ps long, during which time the system was allowed to equilibrate. This was followed by 15 ps of dynamics, during which time trajectories were recorded. In both stages, the time step was set to 1 fs.

Calculation of the Overall Correlation Time. The HYDRONMR program (*30*) was used to estimate the expected overall rotational correlation time and rotational diffusion tensor elements based on the published Adx^o and Adx^r structures. The correlation times, combined with experimentally determined ^{15}N R_2/R_1 ratios of oxidized and reduced Pdx (*31*), were used to estimate the atomic element radius (AER) for Adx. The atomic element radius (AER) is an adjustable parameter in HYDRONMR calculations, and the difference between AER and the van der Waals radius can be taken as an estimate of the thickness of the hydration shell. The atomic element radius obtained in this manner was used to calculate rotational correlation times for Adx^o and Adx^r using the recently published NMR structures (*4*). Hydrodynamic calculations yield values for the diagonalized anisotropic diffusion tensor, and the resulting D_x, D_y, and D_z components of this tensor are transformed to the ratio between parallel and perpendicular components, $D_{\mathrm{para}}/D_{\mathrm{perp}}$, where $D_{\mathrm{para}}/D_{\mathrm{perp}} = 2D_z/(D_x + D_y)$. The values of $D_{\mathrm{para}}/D_{\mathrm{perp}}$ obtained in calculations can be taken as the measure of anisotropy, with $D_{\mathrm{para}}/D_{\mathrm{perp}} = 1$ for a molecule that tumbles isotropically. The subroutine *tmest* of the Modelfree software package (*32*) was used to estimate overall rotational correlation times based on the average R_2/R_1 ratio for both forms of Adx and mutants.

RESULTS AND DISCUSSION

Comparison of WT and Mutant Protein Structures. The current NMR data allow us to compare the structures of H56Q and H56R Adx to that of WT Adx. A set of three NMR experiments and ^{1}H 2D NOESY and ^{1}H 2D TOCSY experiments with two mixing times (t_m =10 and 60 ms), which provide through-bond correlations between ^{1}H resonances directly or indirectly coupled, respectively, were obtained for each of the three variants. On the basis of observed NOEs, the overall structures of mutant proteins are similar to the structure of the WT Adx. There are, however, some differences. The most significant difference is the absence in the mutants of two resonances observed in WT Adx at 11.25 and 11.76 ppm. These are assigned in WT Adx to the Ser 88 O$^\gamma$H and His 56 H$^{\delta 1}$, respectively, on the basis of analogy with human Adx in which these resonances were previously assigned (*16*). These assignments were confirmed by NOESY. The absence of the signal from His 56 is of course expected. However, the absence of the signal for Ser 88 O$^\gamma$H in both mutants suggests that the hydrogen-bonding network involving this proton is weakened or absent in the mutants. In WT Adx, this proton is at sufficiently slow exchange with solvent to be observed directly due to a hydrogen bond between the Ser 88 O$^\gamma$H and His 56 N$^\epsilon$ (vide supra) (Figure 1). The N$^\delta$H of His 56 is also involved in a hydrogen bond (to the backbone carbonyl oxygen of Tyr 82). It has been suggested previously (*15*, *16*) that this hydrogen-bonding network has an important role in transmitting any redox-dependent changes from the metal cluster binding loop to the interaction domain. It was recently proposed (*4*) that the His 56 N$^{\delta 1}$H−Tyr 82 C═O hydrogen bond is broken upon cluster reduction, and an NMR-derived structure (PDB entry 1L6V) of the reduced bovine Adx has been described. However, both the Ser 88 H$^\gamma$ and His 56 N$^{\delta 1}$H signals are observed in the spectrum of WT Adx^r, indicating that their protection from exchange (usually an indication of stable hydrogen bonding) is maintained in Adx^r. Furthermore, the extreme downfield ^{1}H shifts of both of these signals are maintained in Adx^r, another strong indicator of hydrogen bonding, and the ^{15}N shift of the His 56 imidazole N$^{\delta 1}$ is only slightly perturbed upon reduction (169.7 ppm in Adx^o, 168.6 ppm in Adx^r). Most importantly, interresidue NOEs to the His 56 N$^{\delta 1}$H resonance that place the imidazole near to the Tyr 82 carbonyl, although weakened by the increased paramagnetism in Adx^r, are still observed upon reduction.

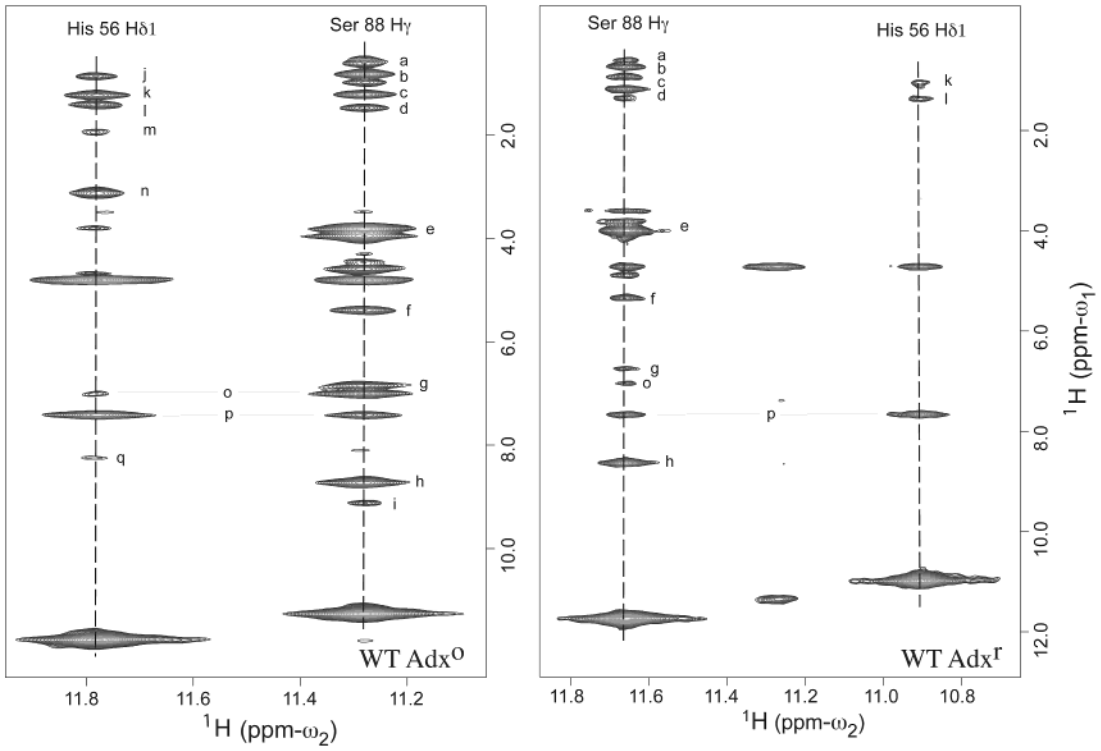

FIGURE 2: 2D ^{1}H NOESY spectra of Adx showing His 56 H$^{\delta 1}$ and Ser 88 H$^{\gamma}$ NOESY connectivities in WT oxidized (Adx^o) and reduced (Adx^r) forms. The NOESY mixing time for the Adx^o spectrum was 80 ms, while the NOESY for Adx^r was acquired using a 50 ms mixing time in order to emphasize features that are more rapidly relaxed by the increased paramagnetism of the Adx^r metal center (see text). Vertical lines indicate ω_2 positions of His 56 H$^{\delta 1}$ and Ser 88 H$^{\gamma}$. Alphabetically marked NOESY cross-peaks are assigned in ω_1 as follows: a, Ile 58 H$^{\delta 1}$; b, Leu 84 H$^{\delta}$; c, Ile 58 H$^{\gamma 1}$; d, Ile 58 H$^{\beta}$; e, Ser 88 H$^{\beta}$; f, Ser 88 H$^{\alpha}$; g, Ser 88 H^N; h, Thr 85 H^N; i, Arg 89 H^N; j, Leu 84 H$^{\delta}$; k, Ala 81 H$^{\beta}$; l, Pro 108 H$^{\gamma}$; m, Pro 108 H$^{\beta}$; n, Pro 108 H$^{\delta}$; o, His 56 H$^{\delta 2}$; p, His 56 H$^{\epsilon 1}$; and q, Tyr 82 H^N.

Taken together, this evidence (summarized in Figure 2) strongly supports the presence of both hydrogen bonds in Adx^r.

The absence or weakening of this hydrogen-bonding network in the two mutants also has thermodynamic consequences. Previous studies of these mutants have shown that His 56 plays a critical role in stabilization of overall Adx structure. On the basis of the results of scanning calorimetric measurements (*19*), replacement of His with a Gln causes a 7 kJ/mol decrease in the net free energy of stabilization. In the case of Arg, the penalty is 5 kJ/mol. This decrease in stability is also apparent from the relative stabilities of these mutants in our experiments.

Other perturbations are indicated by chemical shift differences between mutant and WT Adx, in the sequence between Tyr 82 and Arg 89 in the interaction domain (see Table 1 and Figure 3). On the basis of chemical shift differences, it appears that H56Q Adx is somewhat more perturbed than H56R relative to WT, especially in the case of the Ser 88 amide proton, with absolute chemical shift differences from WT of 0.72 and 0.30 ppm in H56Q and H56R, respectively. For most residues, chemical shifts of amide protons are essentially the same in WT and in both mutants (with chemical shift differences less than 0.1 ppm), indicating that the overall structure is preserved in the mutants. Although some chemical shift changes are observed upon reduction of H56Q and H56R Adx, they are not as pronounced as those observed in WT Adx (Figure 4). This is an indication that replacement of His 56 results in less efficient transmission of redox-dependent structural perturbations in the mutants.

Table 1: ^{1}H Resonance Assignments for the Oxidized Form of WT, H56Q, and H56R Adx for Residues That Exhibit Significant Mutation-Induced Perturbations[a]

resonance	WT Adx^o [b]	H56Q Adx^o	H56R Adx^o
	δ ^{1}H (ppm)		
Ser 28, H$^{\alpha}$	5.77	5.73	5.62
His 56, H$^{\delta 1}$	11.76		
Gln 56, H$^{\epsilon 21}$ and H$^{\epsilon 22}$		6.63, 7.57	
Arg 56, H$^{\epsilon}$			7.60
Ile 58, H^N	8.46	8.37	8.34
Glu 60, H^N	9.18	9.26	9.30
Leu 67, H^N	6.76	6.63	6.64
Met 77, H^N	7.06	not detected	not detected
Gly 83, H^N	8.34	8.37	8.13
Ser 88, H^N	6.88	7.59	7.18
Ser 88, H$^{\alpha}$	5.38	5.87	5.84
Ser 88, H$^{\gamma}$	11.25	not detected	not detected
Arg 89, H^N	9.17	8.91	8.88
	δ ^{15}N (ppm)		
Gln 56, N$^{\epsilon}$		112.54	

[a] Other resonance assignments correspond with those listed in BMRB entry 4566 (see ref *4*). [b] All assignments for WT Adx are taken from ref *4*.

The results of molecular dynamics simulations of the two mutants suggest potential structural perturbations resulting from the mutations. Structures of the two mutants obtained from the simulations were superimposed on the WT Adx structure (Figure 5). Backbone RMSDs relative to WT of 0.66 Å for H56R and 0.94 Å for H56Q Adx were obtained. The differences are localized within the interaction domain, while the hydrophobic cores display essentially no differences between the mutant and WT proteins. The Asp 72−

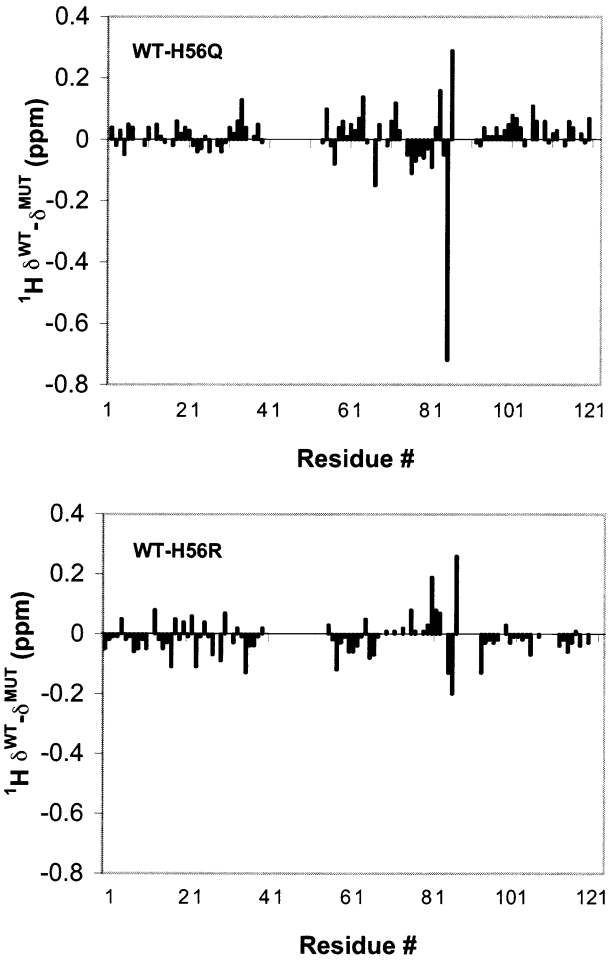

FIGURE 3: Difference between chemical shifts of the amide proton of WT Adx^o and H56Q Adx° (open squares) and amide protons of H56R Adx^o (open diamonds) as a function of residue number. Gaps are due to the lack of assignments in paramagnetically broadened regions of the protein.

Asp 79 helix unravels slightly in simulations of both mutants, ending at Met 77 rather than Asp 79. Resonances corresponding to Met 77 could not be detected in either of the two mutant proteins, which might indicate that Met 77 lies closer to the paramagnetic center in the mutants than in the WT. In simulations of both mutants, perturbations are also observed in the β-turn Ala 81−Leu 84 and in helix Gln 61−Phe 64.

An additional pair of resonances is observed in the region of the ^{1}H, ^{15}N HSQC of H56Q where side-chain NH_2 resonances of glutamines and asparagines are observed. It is reasonable to assign these to the Gln 56 $H^{\epsilon 21}$, $H^{\epsilon 22}$, and $N^{\epsilon 2}$ (Table 1). Furthermore, these resonances show NOESY cross-peaks to the H^N and H^α of Leu 84, the H^N and H^γ of Ile 58, and the H^α of Gly 83. These observations are consistent with the structure of the H56Q mutant obtained from the simulation. We have also tentatively assigned the H^ϵ resonance of Arg 56 in H56R Adx^o, at 7.60 ppm. This signal gives rise to NOESY cross-peaks with Tyr 82 H^N, Ser 88 H^β, and Pro108 H^δ. Again, this agrees with the expected position of this side chain in the H56R mutant from the computationally derived structure.

Redox-Dependent Dynamics of WT Adx Probed by Amide H/D Exchange. Amide proton hydrogen−deuterium (H/D) exchange can provide useful dynamic information on time

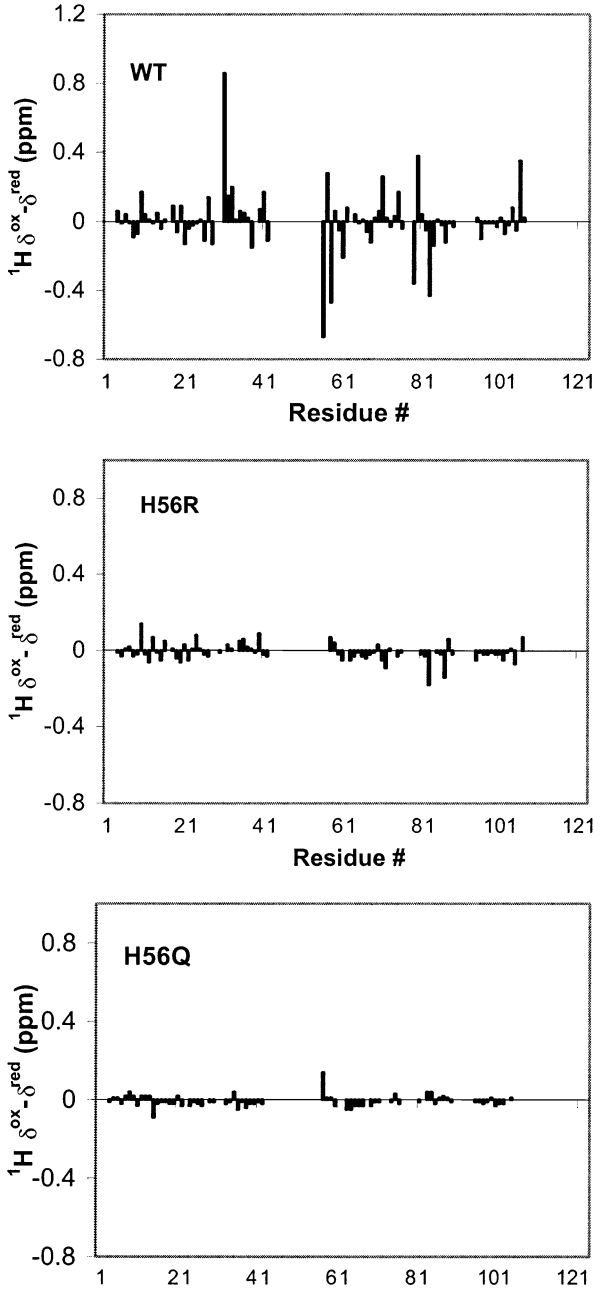

FIGURE 4: Chemical shift difference for amide protons in oxidized and reduced WT (top), H56R (middle), and H56Q (bottom) Adx as a function of residue number. WT Adx exhibits the most pronounced redox-dependent change in chemical shifts, especially within the interaction domain. Gaps are due to the lack of assignments in paramagnetically broadened regions of the protein.

scales 1 ks and longer. Individual peak intensities were followed as a function of exchange time and were fit to a single exponential first-order rate equation. In this manner, rate constants for 29 residues in oxidized and 31 residues in reduced Adx were obtained (Table 2). The remainder of the residues were either exchanging with a rate greater than 1×10^{-3} s^{-1} and are completely exchanged before the first data set has been collected, or exchange so slowly that their intensities do not decay appreciably over the time course of the experiment.

On the basis of H/D exchange rates, it is clear that WT Adx^o is more dynamic than WT Adx^r on the kilosecond time

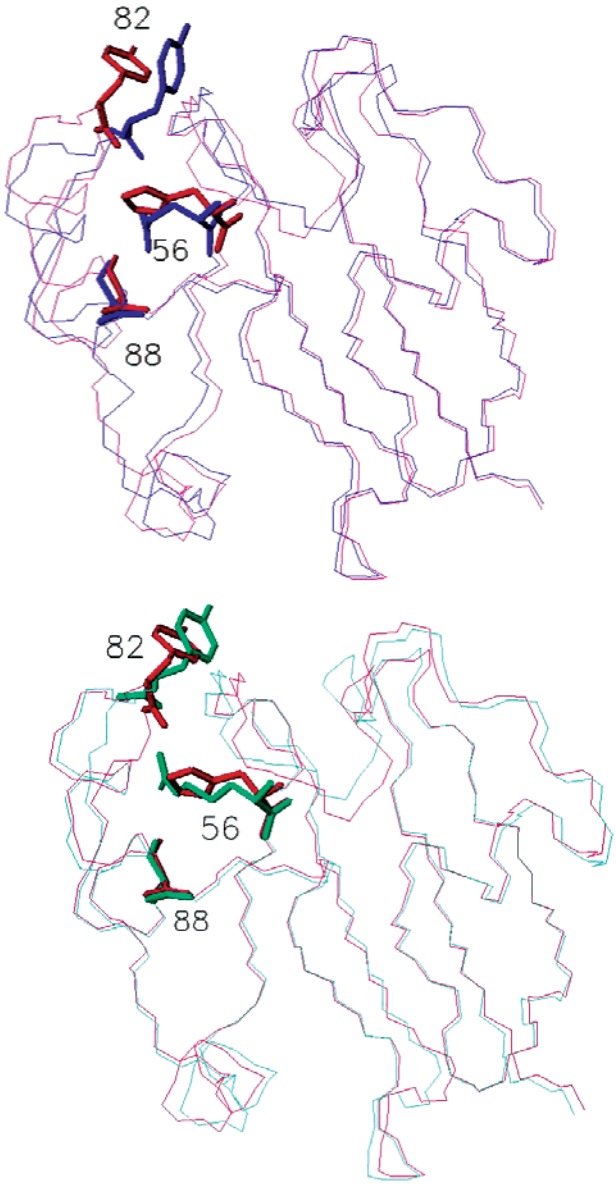

FIGURE 5: Schematic representation of the crystal structure of oxidized Adx (red) overlaid with the minimized model of the H56Q Adx mutant structure (blue), at the top, and overlay of the oxidized Adx crystal structure (red) with the minimized model of the H56R Adx mutant structure (teal), at the bottom. In both cases, residue 56, 82, and 88 side chains are highlighted. The figure is made using MOLMOL (*42*).

scale (see Figure 6 and Table 2). In this respect, bovine Adx is similar to many other simple redox-active metalloproteins, human Adx (*16*), putidaredoxin (Pdx) (*33*), cytochrome b_5 (*34*), and others (*35*). Several regions of the protein are particularly affected. One is a short β-strand close to the metal binding site (residues 18−23), with residue Lys 22 ($k^{ox}/k^{red} = 39.44$) being especially sensitive. Another is the region of irregular structure immediately preceding the metal cluster binding loop, with Leu 38 ($k^{ox}/k^{red} = 22.03$) being the most affected. Leu 38 is also one of the residues for which the large differences in chemical shift between two oxidation states are detected (*4*). As was the case with Pdx (*31*, *33*) the interaction domain of Adx is also strongly affected by redox changes. In this region, Leu 80 ($k^{ox}/k^{red} = 68.30$) is most affected. This amide proton is within hydrogen

Table 2: Rate Constants for Amide Proton H/D Exchange for Oxidized and Reduced WT Adx, Determined at 290 K, Calculated Protection Factors, and Ratio of Rate Constants for Two Forms of the Protein

residue	k^{ox} (s^{-1}) × 10^{-5}	$P^{ox} \times 10^4$	k^{red} (s^{-1}) × 10^{-5}	$P^{red} \times 10^4$	k^{ox}/k^{red}
Ile 7	3.35	26.01	0.99	87.45	3.36
Thr 8	6.44	1.92	2.54	4.87	2.54
His 10	0.44	73.66	0.42	78.07	1.06
Asn 13	4.94	11.13	3.10	17.77	1.60
Glu 17	fast[a]	0.98	60.60	1.61	1.65
Leu 19	2.72	38.58	1.98	5.31	1.38
Thr 21	2.20	51.04	0.36	312.3	6.12
Lys 22	7.65	30.00	0.19	11.84	39.44
Gly 23	11.40	8.18	6.54	18.13	1.74
Lys 24	28.30	0.76	11.60	1.841	2.43
Ile 25	7.29	26.17	slow[b]	190.8	7.29
Ser 28	9.91	1.364	8.52	1.59	1.16
Leu 29	fast[a]	57.57	17.40	87.18	5.75
Gln 35	3.02	33.76	2.00	54.93	1.52
Asn 36	11.30	3.70	6.93	81.40	1.63
Leu 38	22.00	19.41	slow[b]	34.97	22.03
Glu 60	14.20	8.65	7.89	7.31	1.80
Phe64	0.26	0.77	0.31	1.42	0.84
Lys 66	17.50	18.01	9.54	53.78	1.84
Leu 67	8.82	4.36	2.95	4.13	2.99
Glu 73	3.64	34.46	3.84	22.18	0.95
Glu 74	4.94	20.11	7.67	20.18	0.64
Asp 76	7.90	0.58	0.79	1.55	10.04
Met 77	23.32	13.01	8.69	79.95	2.68
Leu 78	3.86	7.52	0.63	51.37	6.15
Leu 80	6.83	1.45	slow[b]	4.06	68.30
Tyr 82	fast[a]	2.99	35.70	5.02	2.80
Thr 85	7.85	15.94	4.69	131.4	1.67
Ser 88	9.73	9.83	1.18	47.32	8.24
Arg 89	4.15	0.12	0.86	0.95	4.81
Cys 95	fast[a]	55.83	12.70	53.39	7.87
Met 100	0.69	3.09	0.73	24.20	0.96
Asp 101	fast[a]	7.43	12.82	9.89	7.81
Asn 102	6.85	26.01	5.08	87.45	1.33

[a] Fast exchanging amide proton with $k > 1 \times 10^{-3}$ s^{-1}. [b] Amide proton in slow exchange with $k < 1 \times 10^{-6}$ s^{-1}.

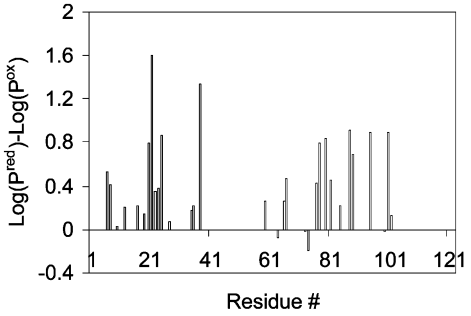

FIGURE 6: Difference of logarithms of protection factors for reduced and oxidized Adx as a function of residue number. Only those residues for which exchange rates could be determined were taken into account.

bond distance of the Met 77 carbonyl oxygen, and this hydrogen bond becomes more protected upon reduction.

Protection factors, $P = k^{int}/k^{exp}$, have been calculated for all of the residues for which values of rate constants for amide proton exchange were determined. From these protection factors, it is seen that the region that is disordered in the published NMR structure of Adx^r (between residues 72−79 and its surroundings) shows an increased level of protection in Adx^r relative to Adx^o. The apparent disorder in the NMR-derived structure is due to the increased

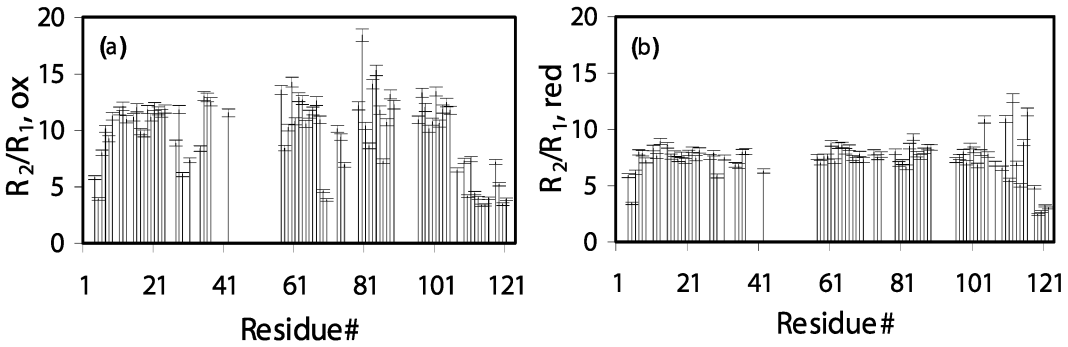

FIGURE 7: R_1, R_2, and R_2/R_1, with uncertainties, are plotted as a function of residue number for oxidized (left) and reduced (right) bovine Adx of all spectrally resolved backbone NH groups. Gaps are due to the lack of assignments in paramagnetically broadened regions of the protein.

paramagnetism in Adx^r, which makes detection of NOEs involving residues 77 and 78 difficult. As such, this part of the structure was only loosely constrained in structure calculations (*4*). It was suggested that the observed loss of order in the NMR-derived structure in this region upon reduction was due to the loss of the hydrogen bond between His 56 $N^{\delta 1}H$ and the Tyr 82 carbonyl oxygen in Adx^r (*4*). However, the accumulated NMR data presented here (protection factors, chemical shift data) clearly show increased order in Adx^r relative to Adx^o in this region. All of our experimental findings strongly support the continued presence of a hydrogen bond between His 56 $N^{\delta 1}H$ and the Tyr 82 carbonyl oxygen in Adx^r.

^{15}N Relaxation Parameters for WT Adx in Both Oxidation States. Backbone dynamics of WT Adx in both oxidation states were investigated by analysis of ^{15}N relaxation rates. For both bovine Adx^o and Adx^r, ^{15}N longitudinal (R_1) and transverse (R_2) relaxation rates were determined for 80 residues. To characterize dynamics on a per residue basis, a selection criterion based on the analysis of R_2/R_1 ratios was applied. The R_2/R_1 mean was calculated for the residues with $^{15}N\{^1H\}$ NOE values higher than 0.6. Large-amplitude internal motions on a time scale longer than a few hundred picoseconds are predicted if the R_2/R_1 ratio for a given residue is more than one standard deviation below the mean. On the other hand, for residues for which the R_2/R_1 ratio is greater than one standard deviation above the mean, an exchange contribution to R_2 is expected (*37*). On the basis of these criteria we can distinguish between residues that undergo chemical or conformational exchange and those that exhibit a significant contribution of large-amplitude internal motions to their relaxation.

Results of determination of ^{15}N relaxation parameters are shown in Figure 7. In both Adx^o and Adx^r the N-terminal residues exhibit high mobility, with Glu 4, Asp 5, and Lys 6 showing internal motions. High mobility is also observed for C-terminal residues. From Val 107 to the C-terminus, R_2 values are significantly below the mean in both Adx^o and Adx^r. Heteronuclear NOEs could not be measured for most of the residues in this region, indicating increased internal dynamics relative to the rest of the protein. Also, some differences are observed between Adx^o and Adx^r in this region. Except for the last four assigned residues, Asp 119−Asn 123, the degree to which internal motion affects R_2 is considerably less for the C-terminus of Adx^r than in Adx^o. In addition, unlike in Adx^o, several C-terminal residues in Adx^r have R_2/R_1 values one standard deviation above the mean, indicating that they experience a significant contribution from the exchange on the millisecond to microsecond time scale. These residues include Thr 104 (which is part of the last β-strand), Ala 110, Ser 112, and Glu 116. The C-terminal residues of human Adx also become more structured upon reduction (*10*). We note that a number of interresidue NOEs identified only in Adx^r indicate a closer association between the C-terminal peptide and the interaction domain in Adx^r than in Adx^o (see Table 3).

Table 3: Interresidue NOEs Involving C-Teminal Peptide Residues in Adx^r

residue	NOE (residue)	NOE (atom)
Asp 109	Asp 109−Pro 108	H^N-H^α
	Asp 109−Pro 108	H^N-H^β
	Asp 109−Ala 110	H^N-H^N
	Asp 109−Ala 110	H^N-H^β
	Asp 109−Ala 110	$H^\beta-H^N$
	Asp 109−Ser 112	H^N-H^α
	Asp 109−Tyr 82	H^N-H^ϵ
	Asp 109−Tyr 82	$H^\alpha-H^\epsilon$
Ala 110	Ala 110−Val 111	H^N-H^N
	Ala 110−Val 111	$H^\alpha-H^N$
	Ala 110−Val 111	$H^\beta-H^N$
	Ala 110−Tyr 82	$H^\beta-H^\delta$
	Ala 110−Tyr 82	$H^\beta-H^\epsilon$
Val 111	Val 111−Arg 115	$H^\alpha-H^N$
	Val 111−Tyr 82	$H^\beta-H^\epsilon$
Ser 112	Ser 112−Asp 113	$H^\beta-H^N$

Other regions in Adx^o exhibit some contribution of internal motion to their ^{15}N relaxation behavior as well. These include Leu 29, Asp 31, and Val 34 in the α-helix within the hydrophobic core and Ala 69, Ile 70, and Asn 75 in the α-helix of the interaction domain. Leu 80, Gly 83, and Leu 84, in the loop region containing Tyr 82, all have R_2/R_1 values one standard deviation above the mean, suggesting an exchange contribution to R_2. Other residues with exchange contributions include Gln 35, Glu 60, Ser 88, Thr 97, and Asp 101.

The situation is considerably different for Adx^r. First, the number of residues affected either by large-amplitude fast internal motions or by conformational exchange is much lower than in Adx^o. Interestingly, residues 80−86, which experience a significant exchange contribution in Adx^o, are unaffected by exchange in Adx^r. This loop exhibits redox-dependent chemical shift changes, and the hydrogen bond between the carbonyl of Tyr 82 and His 56 $H^{\delta 1}$ is critical for transmitting redox-dependent changes into the interaction domain of Adx (vide infra). This further suppports our

Table 4: Average ^{15}N Relaxation Parameters for WT, H56R, and H56Q Bovine Adx at 290 K and 500 MHz

protein	R_1 (s^{-1}), av	R_2 (s^{-1}), av	NOE, av	R_2/R_1, av
WT Adx^o	1.68 ± 0.30	18.78 ± 2.24	0.86 ± 0.19	11.23 ± 1.25
WT Adx^r	1.84 ± 0.20	14.10 ± 1.34	0.89 ± 0.24	7.71 ± 0.57
H56R Adx^o	1.68 ± 0.18	16.22 ± 3.96	0.80 ± 0.13	9.77 ± 2.43
H56R Adx^r	1.76 ± 0.23	13.34 ± 3.90	0.75 ± 0.20	7.65 ± 2.25
H56Q Adx^o	1.69 ± 0.18	11.38 ± 1.30	0.74 ± 0.09	6.87 ± 0.99
H56Q Adx^r	2.09 ± 0.18	14.22 ± 3.35	not available	6.85 ± 1.69

conclusion that this hydrogen bond is maintained in Adx^r. We conclude that, in general, Adx^r is more ordered, with smaller amplitude motions than Adx^o.

Estimation of the Overall Correlation Time τ_m and Rotational Diffusion Anisotropy. As shown in Table 4 and in Figure 7, there are significant global differences between Adx^o and Adx^r that affect relaxation behavior. ^{15}N R_2 is systematically lower in Adx^r than in Adx^o, resulting in a mean R_2/R_1 ratio significantly lower for Adx^r than Adx^o. This was not the case for Pdx (*30*).

An explanation for this phenomenon is a change in the overall molecular correlation time, τ_m. The R_2/R_1 ratio can be used to estimate τ_m (*32*). After removing values for residues with significant large-amplitude internal motions or exchange contributions from the analysis, the mean R_2/R_1 value is calculated and used to estimate τ_m, as described in Materials and Methods (*32*). Using values of 11.23 and 7.71 as R_2/R_1 ratios for oxidized and reduced Adx, respectively, gave estimates for the overall correlation times τ_m of 12.37 ± 0.78 ns for Adx^o and 9.98 ± 0.42 ns for Adx^r. This represents an ~25% decrease in τ_m for Adx^r relative to Adx^o. This is quite different from Pdx, where τ_m of 8.0 ns for Pdx^o and τ_m of 8.3 ns for Pdx^r were calculated (*31*). The primary structural difference between Pdx and Adx is the absence of the disordered C-terminal peptide in Pdx. The C-terminal peptide of Pdx spends at least some fraction of the time interacting with the rest of the protein in both oxidation states (*38*). We propose that the C-terminal peptide of Adx strongly influences the overall tumbling of the molecule. Since the C-terminal peptide is more disordered in Adx^o, it slows down molecular tumbling disproportionately in Adx^o, resulting in faster R_2 relaxation. The increased ordering of the C-terminal peptide upon reduction increases the tumbling rate, with concomitant decrease in measured R_2 values.

It is also expected that disorder of the C-terminal peptide should result in anisotropic motion in solution. We used computational methods to predict the expected diffusion anisotropy of Adx^o and Adx^r. Starting from atomic coordinates and experimental parameters, HYDRONMR (*30*) was used to predict the anisotropic molecular rotational diffusion tensor, overall correlation time, and ^{15}N R_1, R_2 and heteronuclear NOE values. An adjustable parameter, the atomic radius element (AER), is used to represent the thickness of the hydration shell for the protein plus the average van der Waals radius of heavy atoms present. We used Pdx (which is expected to tumble more isotropically than Adx) as a model to yield a preliminary value for the AER. Using 4.8 Å as a value for the AER of Pdx gave an 8.08 ns value for an overall correlation time and 5.46 as the mean R_2/R_1 ratio, which is in excellent agreement with experimental results of 8 ns and 5.48 (*30*). Using this value for AER in combination with the recently published NMR structures for Adx^o and Adx^r as structural input gives R_2/R_1 ratios that are consistently underestimated for Adx^o and overestimated for Adx^r. To reproduce experimentally obtained R_2/R_1 ratios, AER values of 5.5 Å for Adx^o and 4.6 Å for Adx^r were required. These values gave R_2/R_1 ratios of 11.17 for Adx^o and 7.69 for Adx^r, in good agreement with the experimental values of 11.23 and 7.71. The τ_m values obtained in these calculations, 12.35 and 9.85 ns for Adx^o and Adx^r, respectively, also agree well with those obtained from relaxation data. Calculated average values for ^{15}N relaxation parameters are 1.522 s^{-1} for R_1, 16.949 s^{-1} for R_2, and 0.88 for heteronuclear NOE in case of Adx^o. For Adx^r these values are 1.805 s^{-1} for R_1, 13.889 s^{-1} for R_2, and 0.89 for heteronuclear NOE. These are in good agreement with experimental results, although agreement is better for Adx^r than Adx^o (see Table 4). For Adx^r the resulting D_{para}/D_{perp} is 1.14, which means that the molecule diffuses nearly isotropically. For Adx^o, the corresponding value is 1.36, indicating that Adx^o has significantly increased anisotropy compared to Adx^r. This is attributed to the redox-dependent differences in the C-terminal peptide described above. The more disordered, solvent-exposed C-terminal tail in Adx^o results in increased anisotropy.

As dimerization has been observed in low concentration solutions of Adx^o (*4*, *7*), it is possible that the observed increase in R_2 for Adx^o could be due to dimer formation. Dimerization would result in a significant increase in R_2. It was pointed out by Bernadó et al. that typical AER values are around 3.3 Å, and larger values of this parameter might indicate dimer fomation (*39*). However, an AER larger than 3.3 Å was required for fitting not only the data for Adx^o but the data for both Pdx and Adx^r, neither of which shows evidence for dimer formation in the concentration range at which we performed our experiments (see Supporting Information). The large value for AER may well be due to a more persistent hydration layer of these proteins.

Rates of Amide H/D Exchange for H56Q and H56R Adx in Both Oxidation States. The results of amide exchange studies of H56Q Adx in both oxidation states are given in Table 5. From these data, it is clear that, unlike WT Adx, there are no significant differences between the two oxidation states for H56Q Adx. This provides further evidence that His 56 is responsible for transmitting many of the redox-dependent perturbations in Adx. It is worth noting that even residues not in the interaction domain no longer exhibit redox-dependent dynamic changes, suggesting that the interaction domain is not merely a passive detector of redox-dependent changes but plays a role in stabilizing those differences in other parts of the protein. Comparing overall results for WT and H56Q Adx, it is seen that, out of 97 amide signals detected in the ^{1}H, ^{15}N HSQC spectrum of WT Adx^o, 16 residues remain unchanged over the whole time period of the experiment, 52 amide protons are gone after the first 30 min, and for 31 residues the exact rate constant values were determined (Table 2). For H56Q Adx^o, of the 94 amides resolved in the ^{1}H, ^{15}N HSQC spectrum, 15 remained unchanged, 58 are completely exchanged within the first 30 min, and 21 residues exchange on the time scale detectable by H/D exchange (Table 5). The increase in number of residues that are fully exchanged within 30 min indicates that the mutant has a more dynamic structure than WT. (Complete tables showing exchange behavior of all

Table 5: Rate Constants for Amide Proton H/D Exchange for Oxidized and Reduced H56Q Adx, Determined at 290 K, and Ratio of Rate Constants for Two Forms of the Protein

residue	k^{ox} (s^{-1}) $\times 10^{-5}$	k^{red} (s^{-1}) $\times 10^{-5}$	k^{ox}/k^{red}
Ile 7	6.01	5.73	1.05
His 10	0.68	0.67	1.03
Asn 13	6.92	7.84	0.88
Leu 19	2.47	2.20	1.12
Thr 21	1.82	1.57	1.16
Lys 22	fast[a]	fast[a]	
Gly 23	11.61	8.49	1.37
Ile 25	fast[a]	fast[a]	
Ser 28	15.27	14.58	1.05
Leu 29	slow[b]		
Gln 35	5.61	4.54	1.24
Asn 36	20.45	22.63	0.90
Leu 38	fast[a]	fast[a]	
Phe 59	2.06	2.42	0.85
Glu 60	23.05	30.63	0.75
Phe64	8.20	10.43	0.79
Leu 67	34.58	40.60	0.85
Ile 70	0.65	0.90	0.72
Asn 75	13.20	9.36	1.41
Asn 76	fast[a]	fast[a]	
Leu 78	0.61		
Leu 80	0.43		
Thr 85	11.12	13.06	0.85
Ser 88	slow[b]	slow[b]	
Arg 89	slow[b]	slow[b]	
Cys 95	fast[a]	fast[a]	
Met 100	1.57	1.06	0.94
Asp 101	23.53	27.38	0.86
Asn 102	6.83	7.37	0.93

[a] Fast exchanging amide proton with $k > 1 \times 10^{-3}$ s^{-1}. [b] Amide proton in slow exchange with $k < 1 \times 10^{-6}$ s^{-1}.

residues for both WT and H56Q Adx in both oxidation states are provided in Supporting Information.) This difference is accentuated upon reduction. WT Adx^r has only 44 rapidly exchanging amide protons (out of 94 detected) whereas H56Q Adx^r has 56 (out of 89 detected). H56Q Adx is more dynamic than WT in several regions. Between Lys 22 and Ile 25, residues that have measurable exchange rates in WT Adx are at fast exchange in H56Q. The second region is in the interaction domain, between Glu 68 and Asn 76. Within the α-helix Asp 72−Asp 79, located within the interaction domain, a number of residues have exchange rates that can be measured by H/D exchange in WT, whereas in H56Q Adx these amides exchange rapidly.

H56Q Adx does not exhibit significant redox-dependent behavior, as reflected by H/D exchange and chemical shift behavior. This observation supports the proposed role of His 56 in transmitting redox-dependent changes from the Fe_2S_2 cluster binding loop to the interaction domain.

The limited stability of H56R Adx precludes precise measurements of H/D exchange rates in that mutant, since sample decomposition is significant on the time scale of the measurements. However, qualitative comparisons suggest that there is some minor slowing of amide exchange in H56R Adx^r relative to the oxidized form, with one residue in the interaction domain, Glu 60, showing ~5-fold slowing in H/D exchange rate upon reduction.

Determination of ^{15}N Relaxation Parameters for H56R and H56Q Adx. Relaxation parameters, ^{15}N longitudinal and transverse relaxation rates, and heteronuclear NOEs were measured for both H56R and H56Q Adx in both oxidation states. Due to the decreased stability of mutant proteins, a certain amount of unfolding was detected during the experiments. To account for this, a control ^{1}H, ^{15}N HSQC experiment was done before and after the completion of the experimental series and used to calibrate signal intensities. Results are summarized in Table 4, and complete tables with all determined relaxation parameters are available in Supporting Information. As with WT Adx, the N- and C-terminal ends of both mutants show a significant contribution of large-scale fast internal motions, exhibiting characteristically low values for R_2/R_1 and small heteronuclear NOEs. Several regions that are identified in WT Adx^o as regions with significant fast internal dynamics, regions Leu 29−Val 34, Ala 69−Asn 75, and Leu 80−Thr 85, are also affected in both mutants. For H56R Adx^o, fast internal motions are detected for Thr 20, Ile 25, Asp 31, Val 34, Ala 69, Ile 70, Asp 76, Gly 83, Arg 87, and Ser 88. This changes slightly in H56R Adx^r, since Ser 88 shows no evidence for fast internal motions and Gly 83 is affected by chemical exchange. In H56Q Adx, the number of peaks that are affected by fast internal dynamics is significantly larger than in WT, in both oxidation states. Residues that have R_2/R_1 ratios one standard deviation lower than the average are located primarily in the interaction domain.

Comparison of R_2/R_1 ratios between oxidation states for WT Adx and both mutants shows that the large redox dependence of ^{15}N R_2 relaxation observed in WT Adx is dramatically reduced in the mutants, especially in the case of H56Q Adx. Using the *tmest* subroutine of Modelfree to calculate overall rotational correlation times, τ_m, based on R_2/R_1 ratios, yielded the following results. For H56R Adx^o the overall correlation time was calculated to be 11.4 ± 1.6 and 9.9 ± 1.6 ns for H56R Adx^r, indicating a 15% decrease in the value of τ_m relative to H56R Adx^o. While significantly less than the difference of 25% observed in WT, this suggests that Arg is still capable of transmitting redox-dependent dynamic changes into the interaction domain. The same calculation for H56Q Adx^o and H56Q Adx^r gives τ_m values of 9.32 ± 0.76 and 9.30 ± 1.52 ns, respectively. It is clear that overall tumbling rates of the two mutants are less sensitive to oxidation state than in WT Adx.

CONCLUSION

The goal of the present work is to establish the role of the conserved histidine residue (His 56 in bovine Adx) in modulating redox-dependent changes in structure and dynamics observed in vertebrate-type ferredoxins. His 56 is sequentially adjacent to the metal cluster binding site (with ligands for the metal cluster provided by Cys 46, Cys 52, Cys 55, and Cys 92) and, hence, sensitive to perturbations in that site. The imidazole side chain of His 56 forms the nucleus of the interaction domain and is hydrogen bonded to two residues within the interaction domain, the carbonyl of Tyr 82 and the hydroxyl group of Ser 88. It has been proposed that this hydrogen-bonding network acts as a mechanical linkage that transmits structural and dynamical changes occurring in the metal cluster binding loop to the interaction domain. With this in mind, the backbone dynamics of WT Adx^o and Adx^r were probed using two approaches, one based on following redox dependence of amide proton exchange rates and the other based on measuring the ^{15}N relaxation parameters. These two techniques allow us to establish the presence of the redox-dependent behavior of

WT Adx on two different time scales and, at the same time, to gain insight in potential structural perturbations in Adx caused by the change in cluster oxidation state. We conclude that WT Adx^o is more dynamic than Adx^r, on all of the time scales studied. Previous studies (*4*) suggest that reduction of Adx might result in disruption of the hydrogen bond between His 56 and Tyr 82. However, in the present study we see no evidence for this, and all of our results suggest that this hydrogen bond is maintained in Adx^r and is, in fact, critical for restricting motions in the interaction domain of Adx^r.

The critical role His 56 plays in transmitting redox-dependent changes is underscored by the results of the H/D exchange study of H56Q Adx in both oxidation states. These unambiguously show that the disruption of the hydrogen-bonding network centered on His 56 leads to almost total absence of redox-dependent differences in H/D exchange rates, at least in regions remote from the iron−sulfur cluster. Furthermore, much smaller redox dependence of H^N chemical shifts was observed in H56Q and H56R Adx mutants than in WT Adx, consistent with less efficient transmission of conformational changes in mutants.

Molecular dynamics simulations were used to model the structure of the mutants, starting from the crystal structure of Adx^o. The calculated structures are consistent with NOEs detected to resonances assigned to the mutated residues in NOESY spectra of the mutants. On the basis of the models and the detailed analysis of NMR data, we conclude that the structural perturbations are relatively small and are localized to the region around residue 56. Therefore, observed changes in the behavior of H56Q and H56R Adx, when compared to WT protein, can primarily be attributed to the absence of His 56 and its hydrogen-bonding network.

We have also discovered that the rotational correlation times of WT Adx^o and Adx^r differ considerably. The τ_m for Adx^o and Adx^r are determined to be 12.37 and 9.98 ns, respectively. While a small but consistent difference of correlation times between Pdx^o and Pdx^r was observed (*31*), the differences between Adx^r and Adx^o are considerably larger. Evidence presented here together with previously published results (*6*, *7*, *10*) indicates that the C-terminal peptide of WT Adx^o is highly disordered in solution. Upon reduction, the C-terminal peptide becomes more ordered, and we suggest that this increased order is reflected in the significantly reduced correlation time for Adx^r. Although all of the amides of residues in the C-terminal peptide are in fast exchange in both oxidation states, the observation of interresidue NOEs that connect the C-terminal peptide to the interaction domain in Adx^r but not in Adx^o further supports a more compact structure for the C-terminus upon reduction.

As noted above, the redox dependence of interactions between Adx and cognate cytochrome P450s is not as pronounced as in the bacterial $Pdx-P450_{cam}$ interaction (*13*) or, for that matter, as in the interactions of Adx and AdR (*11*, *12*). It is not yet clear whether the redox-dependent dynamic and structural changes detected in Adx are involved in modulating interactions with P450 or if other mechanisms of control not available to the prokaryotic analogues are more important than local structural and dynamic changes in modulating binding and electron transfer between Adx and its redox partners.

ACKNOWLEDGMENT

The authors thank Sara Barkow for help in preparing some of the samples used in this work. Valuable suggestions by Wolfgang Reinle on the purification protocol are gratefully acknowledged.

SUPPORTING INFORMATION AVAILABLE

Complete H/D exchange data for oxidized and reduced WT and H56Q Adx and concentration−line width measurements relevant to dimer formation as well as MD-calculated structures for H56R and H56Q Adx. This material is available free of charge via the Internet at http://pubs.acs.org.

REFERENCES

1. Orme-Johnson, N. R. (1990) *Biochim. Biophys. Acta 1020*, 213−231.
2. Lambeth, J. D., Seybert, D. W., and Kamin, H. (1979) *J. Biol. Chem. 254*, 7255−7264.
3. Hanukoglu, I., and Jefcoate, C. R. (1980) *J. Biol. Chem. 255*, 3057−3061.
4. Beilke, D., Weiss, R., Loehr, F., Pristovsek, P., Hannemann, F., Bernhardt, R., and Rueterjans, H. (2002) *Biochemistry 41*, 7969−7978.
5. Becker, V., and Bernhardt, R. (1997) *J. Biol. Chem. 272*, 4883−4888.
6. Müller, A., Müller, J. J., Müller, Y. A., Uhlmann, H., Bernhardt, R., and Heinemann, U. (1998) *Structure 6*, 269−280.
7. Pikuleva, I. A., Tesh, K., Waterman, M. R., and Kim Y. (2000) *Arch. Biochem. Biophys. 373*, 44−55.
8. Müller, J. J., Müller, A., Rottmann, M., Bernhardt, R., and Heinemann, U. (1999) *J. Mol. Biol. 294*, 501−513.
9. Overington, J. P. (1992) *Curr. Opin. Struct. Biol. 2*, 394−401.
10. Xia, B., Volkman, B. F., and Markley, J. L. (1998) *Biochemistry 37*, 3965−3973.
11. Lambeth, J. D., and Pember, S. O. (1983) *J. Biol. Chem. 258*, 5596−5602.
12. Grinberg, A. V., Hannemann, F., Schiffler, B., Muller, J., Heinemann, U., and Bernhardt, R. (2000) *Proteins 40*, 590−612.
13. Pochapsky, T. C., Kostic, M., Jain, N., and Pejchal, R. (2001) *Biochemistry 40*, 5602−5614.
14. Beckert, V., Schrauber, H., Bernhardt, R., Van Dijk, A. A., Kakoschke, C., and Wray, V. (1995) *Eur. J. Biochem. 231*, 226−235.
15. Miura, S., and Ichikawa, Y. (1991) *Eur. J. Biochem. 197*, 747−757.
16. Kostic, M., Pochapsky, S. S., Obenauer, J., Mo, H., Pagani, G. M., Pejchal, R., and Pochapsky, T. C. (2002) *Biochemistry 41*, 5978−5989.
17. Kakuta, Y., Horio, T., Takahashi, Y., and Fukuyama, K. (2001) *Biochemistry 40*, 11007−11012.
18. Miura, S., Tomita, S., and Ichikawa, Y. (1991) *J. Biol. Chem. 266*, 19212−19216.
19. Burova, T. V., Beckert, V., Uhlmann, H., Ristau, O., Bernhardt, R., and Pfeil, W. (1996) *Protein Sci. 5*, 1890−1897.
20. Uhlmann, H., Beckert, V., Schwarz, D., and Bernhardt, R. (1992) *Biochem. Biophys. Res. Commun. 188*, 1131−1138.
21. Wishart, D. S., Bigam, C. G., Holm, A., Hodges, R. S., and Sykes, B. D. (1995) *J. Biomol. NMR 5*, 332.
22. Cavanagh, J., Plamer, A. G., Wright, P. E., and Rance, M. (1991) *J. Magn. Reson. 91*, 429−436.
23. Kay, L. E., Keifer, P., and Saarinen, T. (1992) *J. Am. Chem. Soc. 114*, 10663−10665.
24. Shaka, A. J., Barker, P. B., and Freeman, R. (1985*) J. Magn. Reson. 52*, 335−338.
25. Raiford, D. S., Fisk, C. L., and Becker, E. D. (1979) *Anal. Chem. 51*, 2050−2051.
26. Kay, L. E., Torchia, D. A., and Bax, A. (1989) *Biochemistry 28*, 8972−8979.
27. Farrow, N. A., Muhandiram, R., Singer, A. U., Pascal, S. M., Kay, C. M., Gish, G., Shoelson, S. E., Pawson, T., Forman-Kay, J. D., and Kay, L. E. (1994) *Biochemistry 33*, 5984−6003.

28. Piotto, M., Saudek, V., and Sklenar, V. (1992) *J. Biomol. NMR 2*, 661−665.
29. Bai, Y., Milne, J. S., Mayne, L., and Englander, S. W. (1993) *Proteins: Struct., Funct., Genet. 17*, 75−86.
30. García de la Torre, J., Huertas, M. L., and Carrasco, B. (2000) *J. Magn. Reson. 147*, 138−146.
31. Sari, N., Holden, M. P., Mayhew, M. P., Vilker, V. L., and Coxon, B. (1999) *Biochemistry 38*, 9862−9871.
32. Mandel, A. M., Akke, M., and Palmer, A. G. (1995) *J. Mol. Biol. 246*, 144−163.
33. Lyons, T. A., Ratnaswamy, G., and Pochapsky, T. C. (1996) *Protein Sci. 5*, 627−639.
34. Dangi, R., Blankman, J. I., Miller, C. J., Volkman, B. F., and Guiles, R. D. (1998) *J. Phys. Chem. B 102*, 8201−8208.
35. Mo, H., Pochapsky, S. S., and Pochapsky, T. C. (1999) *Biochemistry 38*, 5666−5675.
36. Bai, Y., Milne, J. S., Mayne, L., and Englander, W. S. (1993) *Proteins: Struct., Funct., Genet. 17*, 75−86.
37. Clore, G. M., Driscoll, P. C., Wingfield, P. T., and Gronenborn, A. M. (1990) *Biochemistry 29*, 7387−7401.
38. Pochapsky, T. C., Ratnaswamy, G., and Patera, A. (1994) *Biochemistry 33*, 6433−6441.
39. Bernadó, P., García de la Torre, J., and Pons, M (2002) *J. Biomol. NMR 23*, 139−150.
40. Wishart, D. S., Sykes, B. D., and Richards, F. M. (1992) *Biochemistry 31*, 1647−1651.
41. Wishart, D. S., and Sykes, B. D. (1994) *J. Biomol. NMR 4*, 171−180.
42. Koradi, R., Billeter, M., and Wüthrich, K. (1996) *J. Mol. Graphics 14*, 51−55.

BI034500R